Published in final edited form as:
Biomacromolecules. 2011 May 9; 12(5): 1686–1696. doi:10.1021/bm200062a.

Regulation of Silk Material Structure by Temperature-Controlled Water Vapor Annealing

Xiao Hu[1], **Karen Shmelev**[1], **Lin Sun**[2], **Eun-Seok Gil**[1], **Sang-Hyug Park**[1], **Peggy Cebe**[3], and **David L. Kaplan**[1,2,*]

[1] Department of Biomedical Engineering, Tufts University, 4 Colby Street, Medford, MA 02155, USA

[2] Department of Chemical and Biological Engineering, Tufts University, 4 Colby Street, Medford, MA 02155, USA

[3] Department of Physics and Astronomy, Tufts University, 4 Colby Street, Medford, MA 02155, USA

Abstract

We present a simple and effective method to obtain refined control of the molecular structure of silk biomaterials through physical temperature-controlled water vapor annealing (TCWVA). The silk materials can be prepared with control of crystallinity, from a low content using conditions at 4°C (alpha-helix dominated silk I structure), to highest content of ~60% crystallinity at 100°C (beta-sheet dominated silk II structure). This new physical approach covers the range of structures previously reported to govern crystallization during the fabrication of silk materials, yet offers a simpler, green chemistry, approach with tight control of reproducibility. The transition kinetics, thermal, mechanical, and biodegradation properties of the silk films prepared at different temperatures were investigated and compared by Fourier transform infrared spectroscopy (FTIR), differential scanning calorimetry (DSC), uniaxial tensile studies, and enzymatic degradation studies. The results revealed that this new physical processing method accurately controls structure, in turn providing control of mechanical properties, thermal stability, enzyme degradation rate, and human mesenchymal stem cell interactions. The mechanistic basis for the control is through the temperature controlled regulation of water vapor, to control crystallization. Control of silk structure via TCWVA represents a significant improvement in the fabrication of silk-based biomaterials, where control of structure-property relationships is key to regulating material properties. This new approach to control crystallization also provides an entirely new green approach, avoiding common methods which use organic solvents (methanol, ethanol) or organic acids. The method described here for silk proteins would also be universal for many other structural proteins (and likely other biopolymers), where water controls chain interactions related to material properties.

Keywords

silk; water vapor annealing; Enzyme degradation; stem cells

*Corresponding author: david.kaplan@tufts.edu.

Supporting Information Available: Confocal microscopy images of hMSC attachment to the water annealed silk films at 60 minutes and 3 days. This material is available free of charge via the Internet at http://pubs.acs.org.

Introduction

Protein-solvent interactions are complicated phenomena involving many factors such as temperature, pressure, internal stresses, initial state of the protein (*e.g*., volume, molecular weight, initial crystallinity) and solvent (e.g., diffusion, swelling, chemistry) [1–14]. Water is the most important solvent of proteins in nature. Water molecules plasticize protein structures with hydrogen bonds, and also promote solvent-induced crystallization [3–12]. Water molecules disrupt intermolecular cohesive forces between protein chains [3–6], reduce steric hindrance for movement and reorientation [3–6], and thus enhance chain mobility of non-crystalline domains in proteins [3–6]. Therefore, a large reduction in the glass transition temperature (T_g) (*eg*. from ~180°C for dried silk protein to less than 25°C with 25 wt% moisture content [14]) becomes favorable in a protein-water system. Below the new lower T_g, protein molecular motions are still restricted to local side chain rotations, and backbone vibrations. Annealing a crystallizable protein above the new lower T_g provides sufficient thermal energy for large-scale molecular motion of protein chains, therefore their crystallization occurs kinetically [3]. Typically, an increase of holding temperature above the T_g corresponds to an increase in the kinetics of cold crystallization in proteins, which results in an increase in both the crystal packing rate and the final equilibrium crystallinity [1–4]. Before crystallization, most proteins quickly dissolve in a small amount of liquid water. Therefore, a method is needed to regulate the interaction of proteins and water molecules, through which one can promote protein crystallization during interaction with water molecules, but avoid possible dissolution.

In the present work we demonstrate a new physical approach to control the structure of fibrous proteins through temperature-controlled water vapor annealing (TCWVA). This non-chemical, relatively simple approach using a full aqueous-based method allows one accurately to control the mechanics, thermal stability, enzyme degradability, and stem cell interactions of protein materials, through control of structural features. This green method represents a significant improvement in the fabrication of protein-based biomaterials, in contrast to widely used chemical-induced crystallization and cross-linking methods including treatments with methanol, ethanol, or organic acids [15–17].

Silk fibroin protein from the *Bombyx mori* silkworm was selected as a typical model of a structural protein biomaterial, and was studied in detail. Silk fibroin is a protein material studied in tissue engineering, biomedical devices, and for drug release. Patterned films [18,19], thin films [20,21], blend films [22–24], sponge tissue scaffolds [25,26], nanofibers [27,28], microspheres [29,30], nanoparticles, [31] and different gels including hydrogels [32], electro-gels [33,34], and vortex gels [35] have been studied in the past decade, allowing the transition of this biopolymer from the traditional textile industry to a broad range of biomedical applications. Two major structural models, termed silk I and silk II, have been reported for silk fibroin [36–40]. Silk I refers to the complex helix-dominated structure existing within the silkworm gland just before spinning, which is significantly different from the soluble random-coil dominated silk protein conformation of uncrystallized silk [40]. Silk II is the insoluble anti-parallel beta-sheet crystal conformation, which forms after the spinning of silk fibers from the spinneret of the silkworm. The physical properties of silk fibers, such as mechanical, thermal, optical, and dielectric properties, vary depending on the structure of the silk and on the content of beta-sheet crystals [16–40]. To date, however, several methods are used to induce beta sheet crystallization in silk biomaterials, with the most common based on the chemical change during immersion of the silk into organic solvents such as methanol or ethanol. Through this process, silk can reach beta-sheet (crystalline) content of ~55% (for MeOH) and ~36% (for EtOH) [37,40–42]. The highest beta sheet crystallinity (around 60%) is obtained through steam-autoclaving in which beta-sheets are induced by both high temperature and high

pressure [17,42]. Low beta-sheet content material was obtained by a room-temperature water annealing method [43], which results in ~30% beta sheet content mixed with a large amount of silk I helical structure [40]. An alternative method to obtain silk I films is to control water evaporation rate during the drying process [40].

The above methods often have complicated processing steps, which significantly limit the reproducibility of the final material structural features. Such variability can adversely impact the functional features sought in these materials, from mechanical properties to biological responses. In contrast to the above approaches, a systematic and relatively simple method to control the beta-sheet crystal content in silk structures is presented in this work. The approach avoids all the chemical processes used previously, relying instead on the physical approach of temperature-controlled water vapor annealing. This approach allows the crystal structure in silk materials to be controlled from silk I-like lowest beta sheet content (<15%) to the highest known beta sheet content (~60%) by simply changing the annealing temperature in the process. Furthermore, longer annealing times (>12 hours) provide an approach for dense silk materials to become more uniform in terms of homogenous structure, making it a suitable starting material for any complex format such as patterned films, foams, nanofibers, micro/nano particles, or gels.

Experimental Section

Materials

Silk fibroin preparation has been reported previously [36–38]. Briefly, *B. mori* silkworm cocoons were cut into fourths and boiled in a 0.02 M Na_2CO_3 solution to extract the glue-like sericin proteins [36]. The remaining silk fibroin was rinsed three times in Milli-Q water and dissolved in a 9.3 M LiBr solution at 60°C for 4h, and then dialyzed with distilled water using dialysis cassettes [molecular weight cut-off (MWCO)=3,500] for 2 days to remove LiBr. After centrifugation and filtration to remove insoluble residues, the silk solution was diluted to 1~2 wt% with ion-free distilled water and cast onto polystyrene dishes to form ~15 μm–thick films, and kept in a dry vacuum environment before measurement to avoid structural changes.

Temperature-controlled Water Vapor Annealing Setup

The experimental setup of the temperature controlled water vapor annealing device is shown in Figure 1. In addition, a heatable vacuum desiccator with temperature controller (Precision Scientific Inc, Chicago, IL) was used for the preparation of a large number of samples, based on the data obtained from the Fig. 1 setup. In Fig. 1, a stainless steel tube with an aluminum sample basket on the end was first connected to the cap of a large glass flask. The tube and basket were placed into the large glass flask, where one of the pumping ports was connected to a vacuum pump. A trap was used to make sure that no water entered the vacuum pump, and a switch on the vacuum tube to stop the vacuum pumping. The vacuum was generated by compressed air, and a vacuum level down to around −25 In./HG (−85 KPa) was obtained. The second pumping port on the flask was fixed with an inserted thermometer to monitor the temperature of the water vapor. The flask was filled with enough distilled water to generate water vapor to fill the flask during evaporation with relative humility (RH) larger than 90%, but remain the boiling water did not touch the bottom of the basket. The flask was then put into a temperature controlled oil bath or ice/water cooler, through which all temperature values between 4°C and 150°C were reached in an equilibrium state. The temperature controller was first set at a desired annealing temperature (T_c), until homogenous water vapor was obtained in the flask after several hours. Then the silk protein samples were transferred into the flask. The flask was then sealed and the vacuum pump was switched on for about 5 minutes. Once the flask was filled

with vapor, the vacuum port was turned off to let the homogeneous water vapor anneal the silk samples.

Two sets of samples were used in the study. One set was used to monitor the kinetics of crystallization at different times for each temperature. Samples were taken out periodically for measurements. The second set of samples was used to assess the protein conformation and other properties after 12 hours annealing at each temperature, after which no further crystallization occurred at that temperature. This strategy is effective in inducing a homogenous crystal structure and crystallinity in both inner and outer regions of a complex material like the silk scaffold. After 12h annealing, samples were taken out of the chamber and kept in a dry room temperature vacuum oven for two days to remove surface moisture.

FTIR analysis

Fourier Transform Infrared spectroscopy (FTIR) analysis of the silk films was performed with a Jasco FT/IR-6200 Spectrometer, equipped with a multiple reflection, horizontal MIRacle™ Attenuated Total Reflectance (ATR) attachment (Ge crystal, from Pike Tech., Madison, WI). 128 scans were co-added for each measurement and Fourier transformed employing a Genzel-Happ apodization function to yield spectra with a nominal resolution of 4 cm^{-1}. The wavenumber ranged from 400 to 4000 cm^{-1}. To identify secondary structures in the protein samples from the absorption spectra, we obtained the peak positions of the Amide I region (1595~1705 cm^{-1}) absorption from Fourier self-deconvolution performed by using a Opus 5.0 software (Bruker Optics Corp., Billerica MA), as described previously [37]. The peak absorption bands were assigned as follows: 1610~1625cm^{-1} and 1696~1704cm^{-1} as β-sheet structure [37, 40]; 1640~1650cm^{-1} as random-coil structure [37]; 1650~1660cm^{-1} as alpha-helical bands [37]; and 1660~1695 cm^{-1} as beta turns [37].

DSC analysis

Five mg of each of the water annealed silk samples were encapsulated in aluminum pans and heated in a TA Instruments (New Castle, DE) Q100 Differential Scanning Calorimeter (DSC), with purged dry nitrogen gas flow (50 mL/min), and equipped with a refrigerated cooling system. The instrument was calibrated with indium for heat flow and temperature. Aluminum and sapphire reference standards were used for calibration of the heat capacity. Standard mode DSC measurements were performed at a heating rate of 2 K/min.

Mechanical Analysis

Uniaxial tensile tests were performed on an Instron 3366 testing frame equipped with a 100N capacity load cell and Biopuls™ pneumatic clamps [41]. Silk solution was first cast in Petri-dish and the cast films were cut into rectangular shape films (5 mm in width and 4 cm in length), after which they were treated with TCWVA at different temperatures and then hydrated in 0.1 M phosphate-buffered saline (PBS) for 24h to reach a swelling equilibrium prior to testing. Test samples submerged into a temperature-controlled testing container (Biopuls™) filled with PBS solution (37°C). A displacement control mode with a crosshead displacement rate of 5 $mm \cdot min^{-1}$ was used and the gauge length was 15 mm. The measured width of the gauge region was multiplied by the average specimen thickness (measured by a Carrera Precision™ Digital LCD Caliper Micrometer) in order to convert load data to tensile stress values. The initial elastic modulus, yield stress, and tensile strength were calculated from stress/strain plots [41]. The initial elastic modulus was calculated by using a least-squares (LS) fitting between 0.05N load and 5% strain past this initial load point [41]. The yield strength was determined by offsetting the LS line by 2% strain and finding the data intercept. Ultimate tensile strength (UTS) was determined as the highest stress value attained during the test. Sample sets (n=6) were statistically analyzed by using a Student t-test analysis of means.

Enzyme degradation

Different temperature water vapor annealed films were first cut into samples of approximately equivalent mass (40 ± 5 mg). Then the films were incubated at 37°C in 40 ml of phosphate-buffered saline (PBS) solution containing 3.1 U ml^{-1} protease XIV, an enzyme used to assess the degradation of beta-sheet crystallized silk samples [40, 44–45]. Solutions were replenished with enzyme and sample residues were collected daily. For each type of vapor annealed film, at least 8 samples were used to obtain a statistically significant data. At designated time points the samples were rinsed gently with distilled water three times, and prepared for mass balance assessment after collection through centrifugation. Samples without enzyme but in PBS served as controls.

Scanning Electron Microscopy (SEM)

The morphologies of the different silk films were imaged using a Zeiss Supra 55 VP SEM. Films were first fractured in liquid nitrogen and sputtered with platinum. The cross-sectioned surface images were imaged.

Human mesenchymal stem cells (hMSCs) attachment and proliferation

hMSCs were obtained from bone marrow aspirates (Cambrex Bio Science Walkersville Inc., Walkersville, MD) of a 25-year old healthy male following a procedure described in previous study [22, 44]. For cell attachment, the different silk films (n=8 for each set) were punched out into discs and placed into a same size 96-well, non-tissue culture treated plate. After sterilization with UV light for 48 hours on both surfaces, they were preconditioned with cell culture medium overnight before cell plating. The UV treatment did not alter the secondary structure of the films based on FTIR analysis. hMSCs were trypsinized and re-plated on the silk films at a density of 5,000 cells/well. Cell attachment and spreading on the films was observed after 60 min and 3 days incubation in 5% CO_2 at 37°C. Images were captured by a phase contrast microscope with a TCS SP2 scanner (Leica Microsystems, Manheim/Wetzlar, Germany). The proliferation of hMSCs on the silk films (n=8 for each set) was assessed using alamar blue assay. Alamar blue is a non-toxic dye that measures the metabolic activity of cells by fluorometric analysis (BioSource International, Inc., Camarillo, CA, USA) [44]. High levels of metabolic activity indicate cellular viability and proliferation, and low levels imply cellular toxicity [44]. At each predetermined time point, the cells in culture were incubated with 100 ul 10% alamarBlue™ in culture medium at 37°C for 1 hour, followed by spectrofluorimetric analysis by excitation at 540 nm and measuring fluorescence at 590 nm in a SepectraMax/Gemini Em fluorescence microplate reader (molecular Devices, Sunnyvale, CA, USA). A set of empty wells with alamarBlue™ culture medium was used as background and controls.

Statistical analysis

Statistical differences were determined by a Mann-Whitney U test (Independent t-test, SPSS). Statistical significance was assigned as *$p<0.05$.

Results and Discussion

Crystallization Kinetics of TCWVA Annealing

Figure 1 illustrates the experimental setup of the temperature controlled water vapor annealing device (see Experimental Section). The crystallization kinetics of the water vapor annealed silk fibroin at different temperatures was then studied by FTIR at different annealing times. Figure 2(a) and (b) show typical time-resolved FTIR spectra during water annealing at two temperatures, (a) 25°C and (b) 95°C. The Amide I (1600~1700 cm^{-1}) and Amide II (1450~1600 cm^{-1}) regions were selected to monitor the formation of the beta-

sheet crystals. Initially, both sample sets were in the non-crystalline state, and there was no peak observed in the wavenumber region of 1600~1640 cm^{-1}, which is the main absorbance region of beta-sheet crystal in Amide I [37]. When the annealing time increased, the beta-sheet crystal peak appeared gradually, centered at 1626 cm^{-1}. The random coil peaks (1640~1649 cm^{-1}) and the alpha-helix peak (centered at 1650 cm^{-1}) decreased simultaneously. This result was similar for all sample sets annealed at different temperatures. The tyrosine side chain absorbance in the Amide II region also shifted from 1515 cm^{-1}, indicating the packing of the dense beta-sheet crystals during the vapor annealing process [3]. The increase in the beta-sheet peaks slowed and stopped after longer crystallization times, typically 12 hours, indicating that the maximum crystallization ability of silk fibroin had been reached. All samples annealed at different temperatures (between 4°C and 100°C) shared the same features described above. For the low temperature annealing samples (e.g., 4°C, 25°C, 37°C), a noncrystalline-to-silk I-to-silk II transition was observed. The soluble random coil dominated silk samples were first transformed to the insoluble helix dominated silk I structure during the initial annealing time (e,g., 30 minutes). After this initial period of time, the partial transition of silk I to beta-sheet dominated silk II structure followed with longer vapor annealing time. In addition, the 4°C water vapor annealing only generated a small amount of beta sheet crystal structure (~14%) in the film, resulting in a stable major silk I material after 12h annealing. This could indicate that the 4°C water vapor may not provide sufficient energy to help the silk molecules to pass above the energy barrier of the silk I to silk II transition. For the higher temperature annealed samples (>40°C), the intermediate silk I structure cannot be easily detected, as the beta sheet transition occurs rapidly, within several minutes.

The relative intensity changes of the crystal vibrational band were utilized to monitor the crystallization kinetics of the silk materials annealed at different temperatures [38]. A non-crystalline spectrum in the Amide I region was first recorded at the starting time as baseline. The area difference in the absorbance spectrum (ΔA) between 1600 and 1644 cm^{-1} is due to beta-sheet crystals [38]. Then the relative crystallinity index vs. times at different annealing temperature was obtained as described previously [38]. The final crystallinity was calculated from the curve fitting of the Fourier self-deconvoluted (FSD) spectrum, a method previously detailed in Ref [37] and in Figure 3(b), which was used to normalize the time-dependent kinetic data. Figure 2 (**c**) shows the crystallinity index of silk samples vs. annealing time at different water vapor annealing temperatures: 4°C, 25°C, 37°C, 60°C, 70°C, and 95°C. To demonstrate the differences, a log10 scale was used in the initial 300 minutes for all samples. It was found that with the increase of the vapor temperature, the kinetics of the beta-sheet crystal formation increased gradually, and reached at a maximum after 500 minutes for all samples. For the low temperature (4°C) annealed samples, the crystal index began to increase after 30 minutes, while the samples exposed to the 95°C vapor, obtained ~22% crystallinity after one second. It should be noted that these kinetic data are based on 15 μm-thick silk films. If the thickness and morphology of the silk materials were changed, the kinetics could be different according to the complexity of the material scaffolds. To achieve a stable equilibrium for all types of silk scaffolds, a long-term (>500 mins) well-annealed sample should be used, which will sustain the maximum crystallinity for the water annealing temperature, and thus generate a uniform beta sheet crystallinity and crystal distribution in all parts of the sample. Figure 3(**a**) shows the FTIR spectra of the 12 hour water annealed silk samples at different temperatures: (a) untreated, (b) 4°C, (c) 25°C, (d) 37°C, (e) 50°C, (f) 70°C, and (g) 95°C. It clearly shows that the maximum beta-sheet peak (1626 cm^{-1}) after 12 hours vapor annealing increased with the increase of annealing temperature. The FSD curve fitted FTIR spectra of 4°C and 95°C water annealed silk is provided in Figures 3(**b**) and Figure 3(**c**), respectively. The silk I indicator 1652 cm^{-1} alpha-helix peak (A) [40, 43] was significantly higher than other peaks such as the random coil peaks (R) [37], beta sheet peaks (B) [37], or beta turn peaks (T) [37]. In summary, Figure

3(**d**) plots the calculated crystallinity vs. water vapor annealing temperature for all 12h annealed silk fibroin samples. The lowest crystallinity was found in the 4°C annealed silk I sample (~14%), while the highest crystallinity was around 60%, from the 100°C vapor annealed sample. The curves tended to be sigmoidal, between 4°C and 37°C the crystallinity increased more than 27% from 14% (4°C) to 41% (37°C). The rate of increase in crystallinity slowed down at higher temperatures; from 37°C (41%) to 100°C (60%) annealed samples, fractional crystallinity increase by 0.19. These results indicate that the low temperature water annealing region (less than 40°C) tended to be the most important region for generating silk materials with significantly different properties. Curve fitting of data points in Fig 3(d) results in a equation: $C = a\cdot(1-\exp(-k\cdot T))$, where a=62.59, k=0.028, T is the annealing temperature, and C is the calculated beta-sheet crystallinity. This equation can be generally used to estimate the final crystallinity of silk samples at their annealing temperature in the future.

In addition, other known crystallization methods are summarized in Fig 3(d) using 15 samples in three groups. Group 1 (G1) focused on the pH and thickness effect on silk crystallinity: the black up triangle 1 is the untreated thin film (<15 um) with about 9% primary soluble beta sheet inside [37]; the black up triangle 3 is the untreated thick silk film or scaffold (>50 um), with self-assembled 18% beta sheet inside the film [26, 40], which tended to be only partially soluble in water; the white up triangle 2 is the pH 8 silk particle sample (beta-sheet ~15%) salted out from solution with potassium phosphate [30], while the white up triangles 4 to 5 indicate pH 7 to pH 4 silk particle/aggregates from this study, covering the crystallinity region of 31% to 39% [30]. Group 2 (G2) demonstrates the effects of different chemicals on silk material crystallinity: the black star 6 is the 2-day ethanol treated silk sample, which has a typical crystallinity of 35% [40]; the black diamond 7 is from formic acid treated silk samples, with ~38% beta-sheets obtained by FTIR [47,48]; the white diamonds 8 and 9 correspond to 1–4 days methanol treatment of silk fibroin films, generating 41% to 56% crystallinity [37]. Last, group 3 (G3) lists silk samples with varying crystallinity induced by physical methods: the black x-cross 10 reveals the beta sheet crystallinity of slow drying silk films (~23%) [40], which contained helix structures like those found in silk I; the black cross 11 is the lowest beta sheet content (~26%) measured from sonication-induced silk hydrogels [32]; the white circle 12 to 13 is the crystallinity data from 30°C to 60°C hot solution casting, covering crystallinity of 30% to 39% [49]; the black left triangle 14 is an NaCl salt-induced silk sponge scaffold (measured beta sheet ~45%) [25], and the final black right triangle 15 is from 120°C steam autoclaved silk films, believed to have the highest crystallinity of silk fibroin (~59%) [17, 42], which is similar to the 100°C water annealed silk sample. Table 1 lists structural comparisons of these silk samples from temperature controlled water vapor annealing with samples from other methods used to control material properties.

Enzyme Degradation

Enzyme degradation of the water vapor annealed silk films at different temperatures was studied in vitro. Figure 4(**a**) shows the weight losses of the 12h water vapor annealed silk films, for the annealing temperature: 4°C, 25°C, 37°C, 70°C, and 90°C. The degradation profiles followed a clear trend: with higher water annealing temperature, more beta sheet crystals were formed in the sample, which resulted in a slower degradation upon exposure to the protease. For the first 36h, the degradation rate appeared to be quicker, perhaps due to the degradation of silk I and noncrystalline silk in the films. After 36h, the degradation rate tended to slow down, and reached a quasi-equilibrium state, which could be related to the degradation of silk II beta sheet crystal structures in samples. A silk I dominated 4°C annealed sample can be fully degraded in 36 hours, similar to the silk I slow drying film [40], while a 90°C annealed beta sheet rich sample only degraded ~10% after 3-days of

protease XIV enzyme treatment, which was close to the data obtained with the autoclave-sterilized silk sample [42]. Protease XIV enzyme degradation of methanol-treated silk films was also reported [42]. After incubation in protease XIV solution at 37°C for 24h, weight loss from the methanol-annealed silk films was about 20% [42], close to that observed in the 70°C water annealed sample. To further understand the enzymatic degradation kinetics, fracture cross-sections of silk samples were observed by SEM. Figure 4(b) shows a representative morphology from a 70°C water annealed sample at different degradation times (A. 0 (original); B. 4 h, C.12 h, D. 24 h, E. 36 h, F. 75 h). The original sample had a high density of stacked beta-sheet crystal domains shown as the connected white crystal knob bundles in the SEM image [38,40]. During 4 hours of enzymatic degradation, the noncrystalline domains in the lower edge of the silk samples were first attacked by the enzyme, and many small globular fractures appeared among the remaining scaffold structures. The noncrystalline small globular fractures were then quickly degraded to become small holes after 12 hours. The remaining scaffolds were similar to the crystalline fibrillar structures after enzyme treatment as we have reported previously [38]. The fibrillar structures were further degraded with increasing hole sizes and depths at 24 h, 36 and 75 h, indicating the beta-sheet crystallines are slowly digested by enzymes during the quasi-equilibrium state. Longer enzyme treatment caused break-up of the samples such that no material could be collected for analysis. All of these results indicate that silk films treated by temperature controlled water vapor (4°C~100°C) cover most degradation variations of other silk samples prepared through different treatments, which is an important feature of functional protein scaffold designing for tissue-related studies and devices. Through temperature controlled water vapor annealing, silk samples with controlled degradation rates could be prepared to match tissue regeneration rates for specific needs [42].

Thermal stability

Figure 5 illustrates standard DSC curves for the silk samples treated with TCWVA: water vapor annealed at 4°C, 25°C, 37°C, 70°C, 95°C. An untreated silk sample (Un), a silk fibroin fiber sample (Fiber), and a 2-day methanol treated sample (MeOH) used as controls. All samples were first held at 140°C (below the untreated silk glass transition temperature: T_g=178°C) for 30 minutes to eliminate bound water molecules in the films [4, 37], resulting in the flat baselines seen before the glass transition state without a significant bound water evaporation peak around 80°C in the silk-bound water systems [3,4]. All curves in Fig 6 showed a small endothermic peak/step above 170°C, and a clear degradation peak above 250°C thereafter. The untreated film (Un) also show a non-isothermal crystallization peak around 210°C before degradation [3,4]. The endothermic peak/step above 170°C was due to the glass transitions of the samples and their temperature values increased with the increase of the water annealing temperature, indicating an increase of crystallinity and thermal stability in the samples. After the appearance of the glass transition, the water annealed films immediately started to degrade above 250°C without a crystallization peak, implying that the crystal structure formed in the longer time annealed silk films had reached a stable maximum, and additional thermal energy could not induce significant β-sheet increment during high temperature DSC scanning. The degradation peaks generally moved to a higher temperature with the increase of the water annealing temperature from 253°C in 4°C vapor annealed sample to 273°C for the 95°C annealed sample, indicating greater thermal stability for the higher temperature annealed samples. In addition to the water annealed sample, the MeOH treated sample showed a similar degradation temperature as the 70°C annealed sample, consistent with their similar beta sheet crystallinity compared in Fig 2 (c). The fibroin fiber had the highest degradation temperature, which may relate to its high crystallinity and orientated chain alignment in nature [15,36]. It should be noted that the 4°C, 25°C, and 37°C annealing samples all showed a lower or similar degradation temperature compared with the untreated sample, and multiple degradation peaks were

observed for the 25°C and 37°C annealed samples. As discussed in the FTIR section (Fig 1 and Fig 2), the 4°C treated sample formed major silk I helix in the structure, and for the 25°C or 37°C annealed samples both silk I and silk II structures likely exist in the films. Therefore, the degradation of these samples tended to be complicated, involving thermal degradation of both alpha helix and beta sheet crystals, compared with other beta sheet dominated samples, or the random coil dominated untreated sample. This double peak degradation phenomenon is also consistent with the results from silk I-rich slow-drying film we discussed previously [40], in which the first degradation peak around 250°C was assigned to the silk I structure, while the second peak around 260°C was from the degradation of beta-sheets (silk II).

Mechanical Properties

Representative tensile stress/strain curves at 37°C in a PBS hydrated environment for the different temperature water vapor annealed silk films are shown in Figure 6(**a**). With change of the water annealing temperature, silk samples exhibited variable force vs. axial strain profiles. In general, the increase of the annealing temperature resulted in a higher strain value at a certain stress force, and tended to break faster than the lower temperature annealed samples. This result was expected as it has previously been demonstrated that high temperature annealed silk films have greater beta-sheet content than the low temperature processed films, and the increase of beta-sheet content is often thought to result in enhanced stiffness in dry mechanical tests [11,41]. Figure 6(**b,c,d**) show the calculated values of the modulus of elasticity, yield stress, and tensile strength, respectively, from the sample sets (each $n \geq 6$) in Fig 6(a). The data revealed that high temperature vapor annealed silk films (60°C, 95°C) exhibit significantly ($p^* < 0.05$) more than a two-fold magnitude increase in modulus of elasticity, tensile strength, and yield stress, when compared with the low temperature vapor annealed silk films (4°C to 37°C). Therefore, since the crystallinities of the 37°C WA (41%) and 60°C WA samples (51%) differ by only 10%, this indicates that the presence of more than 41% beta-sheet crystallinity had a significant effect on silk film mechanical properties. Only the 4°C treated sample had a significantly ($p^* < 0.05$) higher elongation ratio (>180%) compared with other samples (85~115%) [40,41]. This result is consistent with the finding in slow drying silk films [40]. Both the 4°C water annealed sample and the slow drying samples has had a dominating silk I helical structure instead of dense beta-sheet crystals. The mechanical data also covered other methods; for example, a methanol treated silk film usually has a Young's modulus of around 17~25 MPa [40,41], and a yield strength close to 2~4 MPa [40,41], which can be obtained from the 37°C~46°C water annealed samples in this study. These results indicated that silk films undergo typical extended plastic deformation and fibroin chain breaks, which can be directly controlled by their structures (silk I/II) and crystallinity through the temperature water vapor annealing method.

Stem cell attachment and proliferation

hMSC attachment and spreading were assessed to evaluate cell responses on the water vapor annealed silk biomaterials. The effect of different levels of crystallinity in the silk films (water annealed at 4°C, 25°C, 70°C, 100°C) on initial cell attachment was investigated at 60 min and 3 days after cell seeding (Supplement Figure 1). After 60 min incubation, a significantly lower number of adhered cells was found for the high temperature annealed sample (76°C and 100°C), compared with the low temperature annealed sample (4°C). The majority of hMSCs acquired an elongated morphology on surfaces of the 4°C and 25°C sample groups. In contrast, most of the attached cells on the surfaces of the 76°C and 100°C samples displayed a spherical morphology, which can lead to reduced viability. These differences in attachment may suggest that the surface of the low crystallinity samples, especially the 4°C silk I sample, favored cell attachment. Viability and proliferation of the

hMSCs was evaluated by alamarBlue™ on the different annealed films (4°C, 25°C, 37°C, 42°C, 50°C, 76°C, and 100°C) for 1–3 weeks (Figure 7). A 20 minute MeOH (crystallinity ~39% by FTIR) and a 20 minute 70% EtOH (crystallinity ~33% by FTIR) treated silk films were used as controls. Cells survived and proliferated on the film surfaces for all samples. The differences of proliferative activity between each week were significant ($p^{**}<0.01$) for the sample sets 4°C, 25°C, 37°C, 42°C, and 50°C. In addition, after 3 weeks, the cell numbers of the high temperature annealed groups (42°C, 50°C, 76°C, and 100°C) were about two-fold higher than that of the low temperature annealed group (4°C, 25°C, and 37°C) ($p^{*}<0.05$). This result indicates that the difference of crystallinity can effect stem cell attachment and proliferation. In all cases the materials were compatible in terms of cell responses.

Mechanism of Temperature Controlled Water Annealing

A model was designed in Figure 8 to explain the mechanism of temperature controlled water annealing. During the annealing of silk samples at different temperatures (4°C to 100°C), water molecules played two roles in this process. First, as small molecules, they penetrate into silk protein chain networks and plasticize the system to become a silk water-bound network with higher chain mobility. This process significantly reduced the glass transition temperature of the protein system. Clear evidence based on a 5% bound water plasticized silk system showed that the T_g had been reduced to around 60~80°C compared to the original glass transition temperature of pure silk (178°C) [3]. Higher humidity (>90% in this study) can bring the glass transition temperature of the system down to room temperature [14], which also can be provided by pumping the vapor from the temperature water annealing container. Second, the water vapor molecules at different temperatures (0~100°C) bring variable thermal energy into the protein-bound water system. According to the thermodynamics of molecules [1], the amount of internal energy (E) in a gas system is directly associated to its temperature (T) by the formula: $E= (f/2)nRT$, where f is the number of degrees of freedom for the gas molecule, n is the molar number of molecules, and R = 8.314 J/K-mole is the idea gas constant. For water vapors, the degrees of freedom f is often considered as 12 [1]. To maintain stable equilibrium, the silk system must absorb most of the thermal energy from free water vapor molecules and transfer it to the silk-water system, through which the system passes above the energy boundary of local vibrations and obtains long range molecular mobility for the silk-water system. The system finally self-assembles to become stacked beta-sheet crystals with variable crystallization rates. The kinetics of crystallization is similar to isothermal cold-crystallization of polymers. For the temperature region just above the glass transition region, the growth rate of the crystals tends to be low, and their final stable crystallinity at equilibrium is also small. Moving to a higher temperature region, the kinetics of crystal growth increase significantly and a higher crystallinity can be reached within a shorter time. This is the reason that silk can reach more than 60% crystallinity in 100°C vapor quickly, but needs at least 9 hours to become equilibrated within a 4°C water vapor environment. SEM was also used to compare and confirm the structural changes of the cross-sectioned silk samples with different structures (Fig 8). As we have previously described [38], an untreated non-crystalline silk sample without stacked beta-sheet crystals is comprised of large pieces of overlapping layers, consisting of bundles of protein with random coil and turn structures. When water vapor treated at 4°C, the overlapping bundles interact with water, and reorganize their micro-domains to become networks dominated by alpha-helix structures. At the knot regions of the networks, many beta-sheet rich fibrillar-like structures (white color in SEM [38]) appear as crystal cross-linkers for the insoluble network [38,40]. With increase of water annealing temperature to 37°C, the amount of beta-sheet crystal grows and covers the entire sample. At 95°C high-temperature water annealing the amount and density of stacked beta-sheet crystal domains increases, which results in large connected crystal bundles in the SEM

images [38,40]. Through this control of temperature, and by using an aqueous-based method, the structure of silk materials can be controlled from an alpha-helix dominated silk I structure to the maximum of beta sheet crystal based silk II structure (Fig 8).

Conclusions

A single systemic method to fully control silk material structure and properties was developed by using temperature-controlled water vapor annealing from 4°C to 100°C. This method can produce any desired structure (from silk I to silk II with controllable beta sheet crystallinity) in silk materials, and thereby provides control over the properties (*e.g.*, mechanical strength, degradation rate, cell response). This control can provide useful options for biomedical applications of silk materials, such as in tissue engineering, drug delivery, or for optical systems based on silk materials. In addition, this simple uniform system is an environmentally friendly, all green treatment. Most significantly, this method could be built into standardized procedures for better control of silk material formation and properties, where control of crystallization is critical to subsequent material properties.

Supplementary Material

Refer to Web version on PubMed Central for supplementary material.

Acknowledgments

The authors thank the NIH P41 Tissue Engineering Resource Center (P41 EB002520) and the Air Force Office of Scientific Research for support of this research. We also acknowledge the assistance of Dr. Qiang Lu for the SEM.

References

1. Flory, PJ. Principles of Polymer Chemistry. Cornell University Press; Ithaca, N.Y: 1953.
2. Rebenfeld L, Makarewicz PJ, Weigmann HD, Wilkes GL. J Macromol Sci R M C. 1976; 15:279–393.
3. Hu X, Kaplan D, Cebe P. Macromolecules. 2008; 41:3939–3948.
4. Hu X, Kaplan D, Cebe P. Thermochim Acta. 2007; 461:137–144.
5. Mo CL, Wu PY, Chen X, Shao ZZ. Vib Spectrosc. 2009; 51:105–109.
6. McPeak, JL. PhD Dissertation. Virginia Polytechnic Institute and State University; 1999. URN: etd-120399–113649
7. Tashiro K, Ueno Y, Yoshioka A, Kobayashi M. Macromolecules. 2001; 34:310–315.
8. Tashiro K, Yoshioka A. Macromolecules. 2002; 35:410–414.
9. Hu X, Lu Q, Sun L, Cebe P, Wang X, Zhang X, Kaplan DL. Biomacromolecules. 2010; 11:3178–3188.
10. Porter D, Vollrath F. Soft Matter. 2008; 4:328–336.
11. Fu CJ, Porter D, Shao ZZ. Macromolecules. 2009; 42:7877–7880.
12. Gupper A, Chan KLA, Kazarian SG. Macromolecules. 2004; 37:6498–6503.
13. Sammon C, Yarwood J, Everall N. Polymer. 2000; 41:2521–2534.
14. Agarwal N, Hoagland DA, Farris RJ. J Appl Polym Sci. 1997; 63:401–410.
15. McGrath, K.; Kaplan, DL., editors. Protein-based materials. Boston: Birkhauser Press; 1996.
16. Motta A, Maniglio D, Migliaresi C, Kim HJ, Wang XY, Hu X, Kaplan DL. J Biomat Sci-Polym E. 2009; 20:1875–1897.
17. Lawrence BD, Omenetto F, Chui K, Kaplan DL. J Mater Sci. 2008; 43:6967–6985.
18. Omenetto FG, Kaplan DL. Nat Photonics. 2008; 2:641–643.
19. Lawrence BD, Cronin-Golomb M, Georgakoudi I, Kaplan DL, Omenetto FG. Biomacromolecules. 2008; 9:1214–1220. [PubMed: 18370418]

20. Wang XY, Hu X, Daley A, Rabotyagova O, Cebe P, Kaplan DL. J Control Release. 2007; 121:190–199. [PubMed: 17628161]
21. Kim DH, Viventi J, Amsden JJ, Xiao JL, Vigeland L, Kim YS, Blanco JA, Panilaitis B, Frechette ES, Contreras D, Kaplan DL, Omenetto FG, Huang YG, Hwang KC, Zakin MR, Litt B, Rogers JA. Nat Mater. 2010; 9:511–517. [PubMed: 20400953]
22. Hu X, Wang X, Rnjak J, Weiss AS, Kaplan DL. Biomaterials. 2010; 31:8121–8131. [PubMed: 20674969]
23. Chen H, Hu X, Cebe P. J Therm Anal Calorim. 2008; 93:201–206.
24. Hu X, Kaplan D, Cebe P. J Therm Anal Calorim. 2009; 96:827–834.
25. Kim UJ, Park J, Kim HJ, Wada M, Kaplan DL. Biomaterials. 2005; 26:2775–2785. [PubMed: 15585282]
26. Lu Q, Zhang XH, Hu X, Kaplan DL. Macromol Biosci. 2010; 10:289–298. [PubMed: 19924684]
27. Zhang XH, Reagan MR, Kaplan DL. Adv Drug Deliver Rev. 2009; 61:988–1006.
28. Jeong L, Lee KY, Liu JW, Park WH. Int J Biol Macromol. 2006; 38:140–144. [PubMed: 16545448]
29. Wang X, Wenk E, Hu X, Castro GR, Meinel L, Wang X, Li C, Merkle H, Kaplan DL. Biomaterials. 2007; 28:4161–4169. [PubMed: 17583788]
30. Lammel AS, Hu X, Park SH, Kaplan DL, Scheibel TR. Biomaterials. 2010; 31:4583–4591. [PubMed: 20219241]
31. Wang XQ, Yucel T, Lu Q, Hu X, Kaplan DL. Biomaterials. 2010; 31:1025–1035. [PubMed: 19945157]
32. Wang XQ, Kluge JA, Leisk GG, Kaplan DL. Biomaterials. 2008; 29:1054–1064. [PubMed: 18031805]
33. Yucel T, Kojic N, Leisk GG, Lo TJ, Kaplan DL. J Struct Biol. 2010; 170:406–412. [PubMed: 20026216]
34. Leisk GG, Lo TJ, Yucel T, Lu Q, Kaplan DL. Adv Mater. 2010; 22:711–715. [PubMed: 20217775]
35. Yucel T, Cebe P, Kaplan DL. Biophys J. 2009; 97:2044–2050. [PubMed: 19804736]
36. Jin HJ, Kaplan DL. Nature. 2003; 424:1057–1061. [PubMed: 12944968]
37. Hu X, Kaplan D, Cebe P. Macromolecules. 2006; 39:6161–6170.
38. Hu X, Lu Q, Kaplan DL, Cebe P. Macromolecules. 2009; 42:2079–2087.
39. Pyda M, Hu X, Cebe P. Macromolecules. 2008; 41:4786–4793.
40. Lu Q, Hu X, Wang XQ, Kluge JA, Lu SZ, Cebe P, Kaplan DL. Acta Biomater. 2010; 6:1380–1387. [PubMed: 19874919]
41. Lawrence BD, Wharram S, Kluge JA, Leisk GG, Omenetto FG, Rosenblatt MI, Kaplan DL. Macromol Biosci. 2010; 10:393–403. [PubMed: 20112237]
42. Park SH, Gil ES, Shi H, Kim HJ, Lee K, Kaplan DL. Biomaterials. 2010; 31:6162–6172. [PubMed: 20546890]
43. Jin HJ, Park J, Karageorgiou V, Kim UJ, Valluzzi R, Cebe P, Kaplan DL. Adv Funct Mater. 2005; 15:1241–1247.
44. Wang X, Zhang X, Castellot J, Herman I, Iafrati M, Kaplan DL. Biomaterials. 2008; 29:894–903. [PubMed: 18048096]
45. Lu Q, Wang XQ, Hu X, Cebe P, Omenetto F, Kaplan DL. Macromol Biosci. 2010; 10:359–368. [PubMed: 20217856]
46. Wang Y, Rudym DD, Walsh A, Abrahamsen L, Kim HJ, Kim HS, Kirker-Head C, Kaplan DL. Biomaterials. 2008; 29:3415–3428. [PubMed: 18502501]
47. Um IC, Kweon HY, Park YH, Hudson S. Int J Biol Macromol. 2001; 29:91–97. [PubMed: 11518580]
48. Um IC, Kweon HY, Lee KG, Park YH. Int J Biol Macromol. 2003; 33:203–213. [PubMed: 14607365]
49. Tretinnikov ON, Tamada Y. Langmuir. 2001; 17:7406–7413.

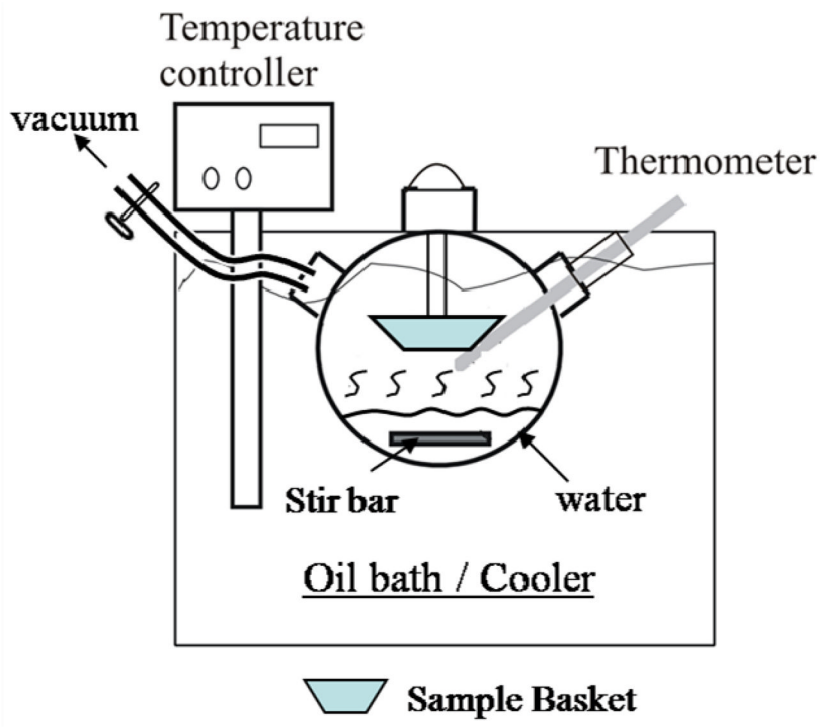

Figure 1.
Diagram of the experimental setup for temperature controlled water vapor annealing.

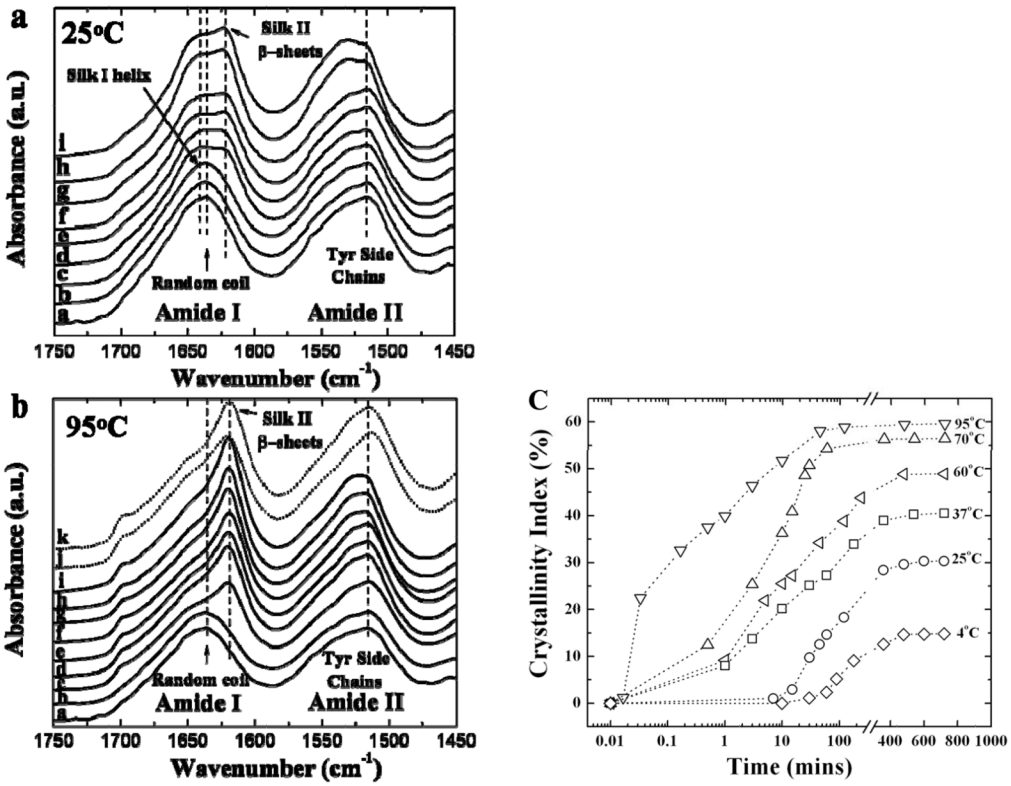

Figure 2.

Typical time-resolved FTIR spectra of silk films during water vapor annealing at two temperatures: (a) 25°C: a. 0 min, b. 7 mins, c. 15 mins, d. 30 mins, e. 45 mins, f. 1 h, g. 2 h, h. 6h, i. 12 h; and (b) 95°C: a. 0s, b. 1s, c. 2s, d. 10s, e. 30s, f. 1 min, g. 3 mins, h. 10 mins, i. 45 mins, j. MeOH treated-control, k. steam-autoclaved-control. (c) Crystallinity index vs. water vapor annealing time at different temperatures: 4°C, 25°C, 37°C, 60°C, 70°C, and 95°C.

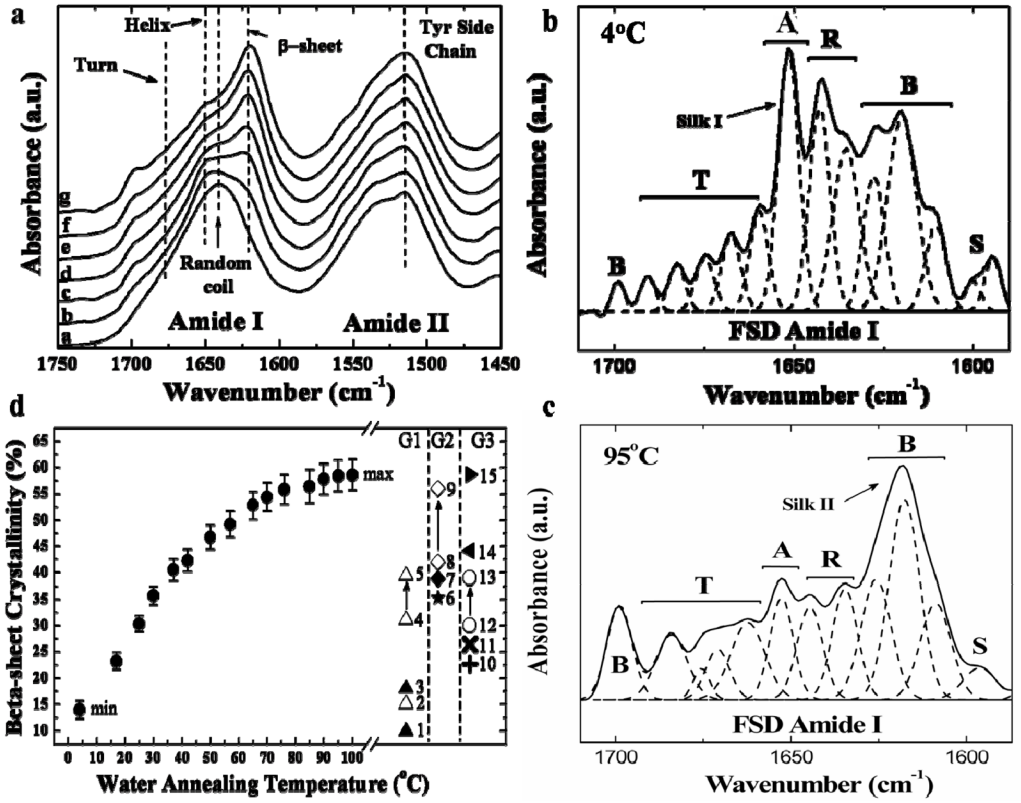

Figure 3.

(a) FTIR spectra of 12 hour water vapor annealed silk samples at different temperatures: a. untreated, b. 4°C, c. 25°C, d. 37°C, e 50°C, f. 70°C, and g. 95°C. (b) Curve fitting example of Fourier self-deconvoluted (FSD) Amide I spectra using the 12h 4°C water annealed sample. The fitted peaks are assigned as side chain (S), beta-sheet (B), random coil (R), alpha helix (A), and turn (T). (c) FSD Amide I spectra of the 12h 95°C water annealed sample. (d) Calculated crystallinity of 12h annealing vs. water vapor annealing temperature for silk fibroin samples, which covered the crystallinity regions from most known methods utilized are on the right. Group 1 (G1): 1. untreated thin film; 2. pH 8 silk particle; 3. untreated thick film; 4 to 5. pH 7 to pH 4 silk particle/aggregates. Group 2 (G2): 6. 2-day ethanol treated film, 7. formic acid treated film; 8 to 9: 1–4 days methanol treated film. And group 3 (G3): 10. slow drying film; 11. sonication induced hydrogel; 12 to 13. 30°C to 60°C hot solution casting; 14. NaCl induced sponge scaffold; 15. 121°C steam autoclaved film.

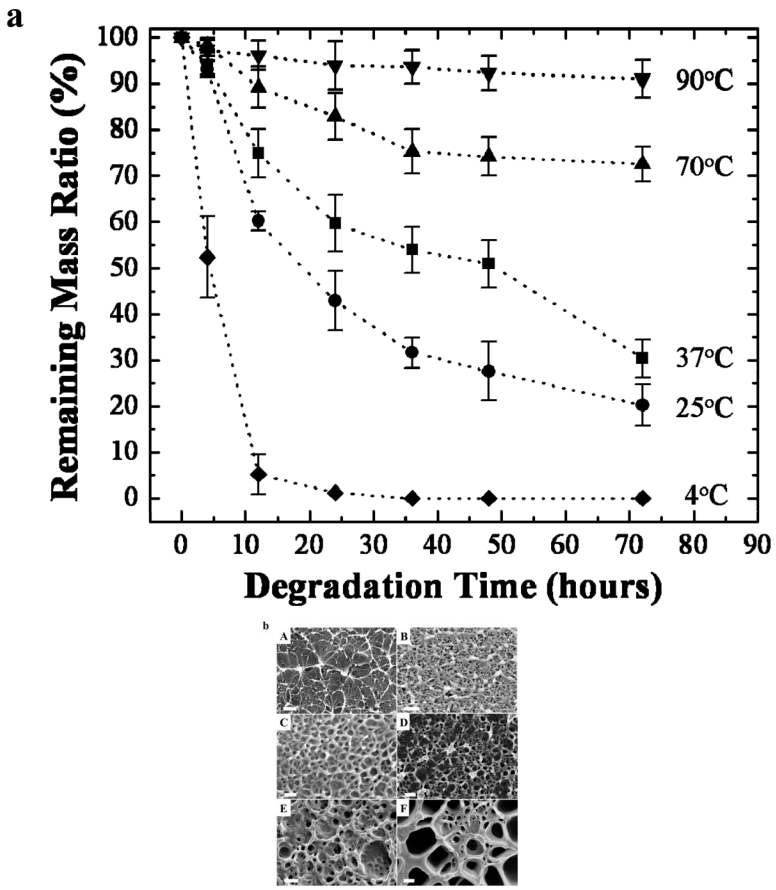

Figure 4.

(a) Three day protease XIV enzymatic degradation study of silk films prepared by 12 h water vapor annealing at variable temperatures: 4°C, 25°C, 37°C, 70°C, and 90°C. n > 8, bars represent standard deviation. (b) SEM morphology of a 70°C water annealed sample at different degradation times: A. 0h (original); B. 4h, C.12h, D. 24h, E. 36h, F. 75h. (Bar length: 200 nm)

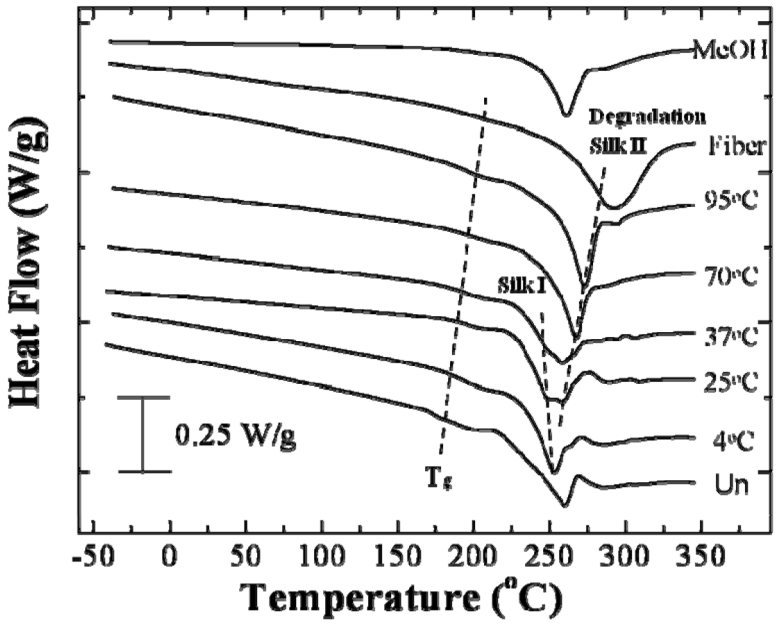

Figure 5.
Standard DSC curves for the silk samples with different treatments: water vapor annealed at 4°C, 25°C, 37°C, 70°C, 95°C. Untreated silk sample (Un), silk fibroin fibers (Fiber), and 2-day methanol treated sample (MeOH) used as controls.

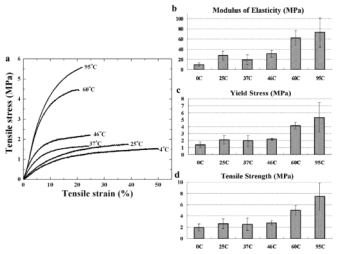

Figure 6.

(a) Representative tensile stress/strain curves for different temperature-water vapor annealed silk films at 37°C PBS hydrated testing, and their calculated (b) modulus of elasticity, (c) yield stress, and (d) tensile strength.

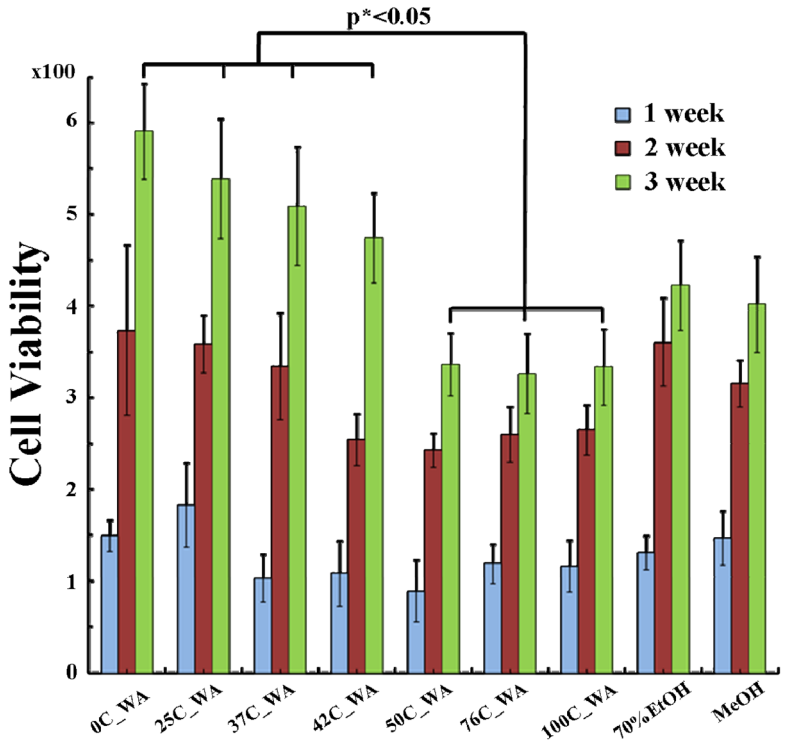

Figure 7.
hMSC proliferation after 1, 2 and 3 weeks on the surfaces of different water annealed films at 4°C, 25°C, 37°C, 42°C, 50°C, 76°C, and 100°C; a 20 min MeOH treated film and a 20 min 70% EtOH treated films utilized as controls.

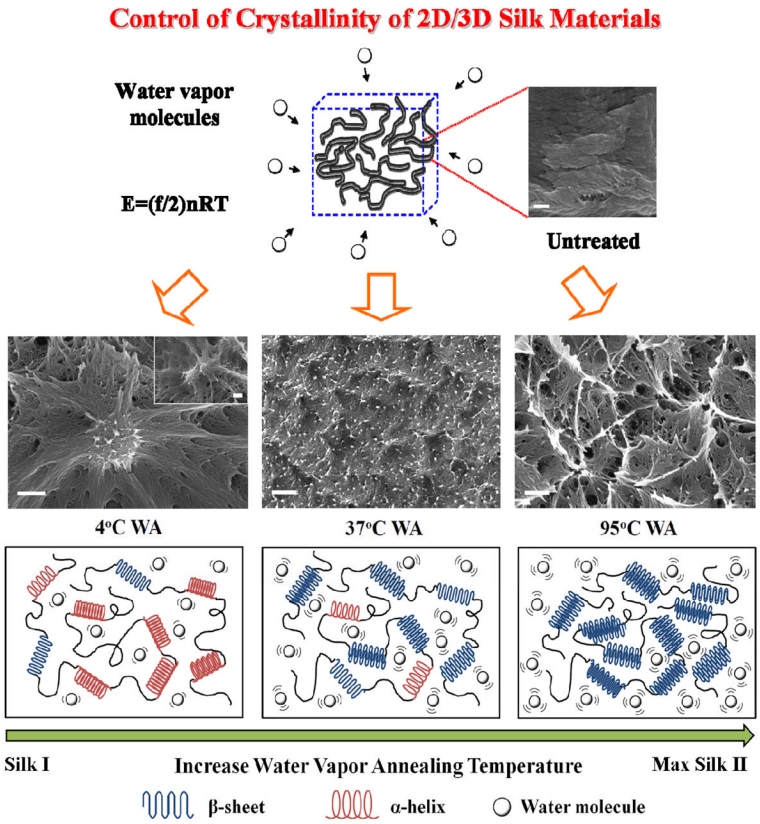

Figure 8.

Mechanisms of temperature controlled water annealing to silk fibroin proteins. Through the variation of vapor temperature, the structure of silk materials can be fully controlled from an alpha-helix dominated silk I structure to the maximum beta sheet silk II structure. (Bar length in SEM images: 200 nm)

Table 1

Structural comparison of silk samples between temperature-controlled water vapor annealing method and previously published methods.

Sample	Beta-sheet Crystallinity (%)*	Traditional method for this crystallinity
4°C WA	14	self-assembled thick samples [Ref 26, 40]; pH 8 solution [Ref 30]
17°C WA	23.2	slow drying [Ref 40]; ultra-sonication [Ref 32]
25°C WA	30.3	pH 7 solution [Ref 30]; 30°C solution casting [Ref 49]
30°C WA	35.7	pH 5–6 solution [Ref 30]; 2-day ethanol treatment [Ref 40];
37–42°C WA	40.5–42.3	pH 4 solution [Ref 30]; 60°C hot solution casting [Ref 49]; formic acid treatment [Ref 47,48]
50°C–57°C WA	46.7–49.2	short term methanol treatment [Ref 37]; high concentrated salts (NaCl) [Ref 25]
65–85°C WA	52.8–56.4	3–4 days methanol treatment [Ref 37]
90°C–100°C WA	57.8–59.6	121°C steam autoclaving [Ref 17,42]

*All numbers have same unit (wt%) with less than ±3% error bar.